Harmful Algae
January 2025, Volume 141 Pages 102761 (12p.)
https://doi.org/10.1016/j.hal.2024.102761
https://archimer.ifremer.fr/doc/00924/103618/

Gonyaulax montresoriae sp. nov. (Dinophyceae) from the Adriatic Sea produces predominantly yessotoxin

Huang Shuning [1, 2], Mertens Kenneth [3], Derrien Amelie [3], David Ophelie [3, 4], Shin Hyeon Ho [5], Li Zhun [6], Cao Xiuyun [7], Cabrini Marina [8], Klisarova Daniela [9, 10], Gu Haifeng [2, *]

[1] School of Marine Sciences, Nanjing University of Information Science and Technology, Nanjing, 210044, China
[2] Third Institute of Oceanography, Ministry of Natural Resources, Xiamen 361005, China
[3] Ifremer, COAST, F-29900 Concarneau, France
[4] Geo-Ocean, UMR 6538,Univ Brest, CNRS, Ifremer, F-29280 Plouzané, France
[5] Division of Fisheries Life Science, Pukyong National University, Busan 48574, Republic of Korea
[6] Biological Resource Center/Korean Collection for Type Cultures (KCTC), Korea Research Institute of Bioscience and Biotechnology, Jeongeup 56212, South Korea
[7] Institute of Hydrobiology, Chinese Academy of Sciences, Wuhan 430072, China
[8] National Institute of Oceanography and Experimental Geophysics, Italy
[9] Medical University, Faculty of Medicine Department of Anatomy, Histology, Cytology and Biology, Pleven, Bulgaria
[10] Institute of Fish Resources, Agriculture Academy, 9000 Varna, Bulgaria

* Corresponding author : Haifeng Gu, email address : guhaifeng@tio.org.cn

Abstract :

Yessotoxin is one of the shellfish toxins leading to mussel farm closures in the Adriatic Sea of Italy. Two putative Gonyaulax spinifera strains GSA0501 and GSA0602 are known as yessotoxins producers, but their identities have remained elusive since 2005. To address this gap, we established five Gonyaulax strains by incubating sediments from the Adriatic Sea and subsequently isolating single cells. Both cyst and theca morphology were examined using light and scanning electron microscopy. In addition, LSU and/or SSU rRNA gene sequences were obtained for all strains. Two strains produce cysts resembling Spiniferites mirabilis and one strain was related to S. scabratus. The other two strains are described as Gonyaulax montresoriae sp. nov., characterized by a high cingular displacement and overhang, along with two unequal antapical spines. Cysts of G. montresoriae are pear-shaped, showing a smooth surface and exclusively gonal processes with perforations at the base, the latter similar to S. lazus. LSU rRNA gene sequence comparison suggests that the G. spinifera strain GSA0501 isolated from the Adriatic Sea in 2005 should also be identified as G. montresoriae. Maximum likelihood and Bayesian inference analyses based on LSU and SSU rRNA gene sequences reveal that G. montresoriae is monophyletic, and close to several toxic strains of presumable Gonyaulax spinifera from the Adriatic Sea and New Zealand, whose taxonomic positions are uncertain. One strain of G. montresoriae was examined for yessotoxin production using LC-MS/MS, and found to produce predominantly yessotoxin at a concentration of 3.0 pg cell-1. Our results highlight the rich diversity and risks associated with Gonyaulax species in the Mediterranean Sea.

Highlights

► *Gonyaulax montresoriae* sp. nov. is described from the Adriatic Sea. ► *Gonyaulax montresoriae* produces predominantly yessotoxin. ► *Gonyaulax montresoriae* produces cysts close to *Spiniferites lazus*. ► Two strains were identified with cysts resembling *Spiniferites mirabilis*.

Keywords : Cysts, Dinoflagellate, Harmful algal bloom, Mediterranean Sea, Spiniferites

1. Introduction

The taxonomy of *Gonyaulax* is notoriously challenging. Their thecal plates are often thick and ornamented by numerous strong reticulations, making it difficult to discern plate boundaries. All *Gonyaulax* species share a plate tabulation of 2pr, 4′*, 6″, 6c, 5–6s, 5‴, 2p, 1⁗ (Carbonell-Moore et al., 2022). They are separated from each other only in the shape and size of cells, the cingular displacement and overhang, the shape of plate 6″, the plate ornamentation, and the number and size of antapical spines (Dodge, 1989; Gu et al., 2022; Kim et al., 2022).

Gonyaulax spinifera has been reported to generate as many as 16 cyst morphotypes, such as *Spiniferites ramosus* and *Nematosphaeropsis labyrinthus* (Rochon et al., 2009). Since then, more and more species have been separated from *G. spinifera* mainly based on cyst morphology and molecular sequences. For instance, *G. lewisiae* (=*G. membranaceae*) was proposed as the equivalent of *Spiniferites membranaceus* (Ellegaard et al., 2003; Head et al., 2024). Later, *Gonyaulax ellegaardiae, G. nezaniae* and *G. pospelovana* were established corresponding to *S. pachydermus, S. bentorii,* and *S. delicatus* like cysts, respectively (Mertens et al., 2015; Gu et al., 2021; Gu et al., 2024).

Yessotoxin (YTX) is a marine polyether toxin that was first isolated from the scallop *Mizuhopecten yessoensis* (Murata et al., 1987). To date, more than 100 analogues of YTX have been reported from dinoflagellates or shellfish; however, most of them have not yet been structurally characterized (Miles et al., 2005; Paz et al., 2008).

They are commonly named as yessotoxins (YTXs) and adriatoxins (ATX) (Ciminiello et al., 1998; Domínguez et al., 2010). Currently, several dinoflagellates including *Protoceratium reticulatum*, *Lingulaulax polyedra* (=*Lingulodinium polyedra*) and a few *Gonyaulax* species are known to produce YTXs (Miles et al., 2005; Armstrong and Kudela, 2006; Rhodes et al., 2006; Pitcher et al., 2019). The EU regulatory limit for YTXs in food is 1 mg YTX equivalents/Kg (Paz et al., 2008). However, Homo-YTX has been considered responsible for the mass mortality of abalone (Pitcher et al., 2019), and the 12 h LC50 values of Homo-YTX to abalone was only 5.1 μg L^{-1} (Liang et al., 2024).

Most reports on the production of YTXs by *Gonyaulax* species have identified the species as *Gonyaulax spinifera*, *G. lewisiae* or *Gonyaulax taylorii*. Two isolates of *G. spinifera* from New Zealand were reported to produce YTX by ELISA method, although the detailed information on the YTXs profiles is not available (Rhodes et al., 2006). Later, two *G. spinifera* isolates from the Adriatic Sea, GSA0501 and GSA0602, produced predominantly YTX and Homo-YTX respectively; both isolates also differed markedly in LSU and SSU rRNA gene sequences and one of them is very close to the toxic *G. spinifera* from New Zealand (Riccardi et al., 2009). Several isolates of *G. spinifera* from the Benguela Current upwelling system that are genetically close to strain GSA0602 from Adriatic Sea, produced homo-YTX as well (Chikwililwa et al., 2019). *Gonyaulax lewisiae* (=*G. membranaceae*) from South Africa was reported to produce homoYTX and 45-hydroxyYTX (Pitcher et al., 2019). In addition, *Gonyaulax taylorii* was reported to produce YTXs but unfortunately a

molecular sequence was not provided (Álvarez et al., 2016). On the other hand, other strains identified as *G. spinifera* and equivalent to *Spiniferites ramosus* do not produce any YTXs (Gu et al., 2021). These non-toxic strains of *G. spinifera* are genetically distinct from the toxic ones, suggesting that they belong to different *Gonyaulax* species.

The northern Adriatic Sea is one of the main areas for shellfish aquaculture in Italy, with mussels as major culture species. YTXs were detected in mussels from the northeastern Adriatic Sea in 1995 for the first time (Ciminiello et al., 1997). Many mussel farms along the Emilia Romagna coast of Italy (northwestern Adriatic Sea) were closed in 2004 because the levels of yessotoxin exceeded EU regulatory limit (Riccardi et al., 2009). Only *Gonyaulax spinifera* was found in the water samples at high densities in 2004, and later, two strains of this species were isolated in 2005 and 2006, producing YTX and Homo-YTX, respectively (Riccardi et al., 2009). These putative toxic *G. spinifera* are genetically different from other *G. spinifera* species and their true identities have remained elusive after two decades. Therefore, we collected sediment samples in Gulf of Trieste, northern Adriatic Sea, to perform germination of potential *Gonyaulax* species. Both cyst and theca morphologies were examined in detail using light microscopy and scanning electron microscopy, and molecular phylogeny was inferred based on LSU and SSU rRNA gene sequences. In addition, a strain of *Gonyaulax* was examined for yessotoxin production by liquid chromatography coupled with tandem mass spectrometry (LC-MS/MS).

2. Material and methods

2.1. Sample collection and treatment

Sediment samples were collected in the Gulf of Trieste, Italy, in 2018 using an Ekman grab sampler (Table 1). Sediment from the top 2 centimeters was gathered and stored in the dark at 4 °C. Approximately 5 g of wet sediment was mixed with 20 mL of sterile-filtered seawater and vigorously stirred to disperse the sediment. The mixture was sequentially passed through 125 µm and 10 µm sieves, and the material collected on the 10 µm sieve was rinsed several times with filtered seawater and collected in a beaker. The residue was transferred to 96-well cell culture plates containing f/2-Si culture medium (Ryther and Guillard, 1962) for germination. The culture conditions were set at 20 °C with a light intensity of 90 µmol $m^{-2}s^{-1}$ under a 12-hour light and 12-hour dark cycle (referred to as standard culture conditions). Emergent cells were observed and isolated using an inverted Eclipse TS100 microscope (Nikon, Tokyo, Japan) with a micropipette to establish five strains (Table 1). Some of these strains produced cysts in culture spontaneously.

2.2. Light microscopy (LM)

A Zeiss Axiocam HRc digital camera was used with the Zeiss Axiocam Imager optical microscope (Zeiss, Göttingen, Germany) to observe and capture images of cysts and motile cells. The size of the cysts and vegetative cells was measured from the captured images. The cells were stained with a 1:100,000 dilution of SYBR Green (Sigma Aldrich), and their nuclear shape, position, and chloroplast distribution within

the cells were observed and documented using the Zeiss-38 filter set (excitation BP 470/40, beam splitter FT 495, emission BP 525/50) on the optical microscope.

2.3. Scanning electron microscopy (SEM)

For SEM observations, 2 mL of mid-exponential batch cultures of strain TIO1290 were fixed with Lugol's Iodine solution (4% final concentration) at room temperature and then rinsed by centrifugation with deionized water. After rinsing, samples were dehydrated, critical point dried, and examined following standard protocols (Gu et al., 2021). Plate labeling follows the Kofoidian system (Kofoid, 1911), except for the sulcal plate labeling, which follows Carbonell-Moore et al. (2022).

2.4. PCR amplifications and sequencing

Single cells of five *Gonyaulax* strains were isolated and washed several times with sterile distilled water. They were lysed by gentle pressing the coverslip under the inverted microscope and pipetted into a PCR tube for templates. Various regions of rRNA genes including the SSU, partial LSU (D1–D6) and ITS1–5.8S–ITS2 were amplified using primer pairs specified previously and following standard protocols (Gu et al., 2021).

2.5. Sequence alignment and phylogenetic analyses

The newly obtained LSU and SSU rRNA gene sequences were compared with those of *Gonyaulax* species and related taxa in the NCBI database. MAFFT v7.110 (Katoh and Standley, 2013) online program (http://mafft.cbrc.jp/alignment/server/) was used for sequence alignment with the default settings and checked manually using

BioEdit v7.0.5 (Hall, 1999). Maximum likelihood (ML) analysis was performed using raxmlGUI v1.5 (Silvestro and Michalak, 2012) with the GTR+G model with 1000 bootstrap replicates (using the 'ML + rapid bootstrap' option). For Bayesian inference (BI), the program jModelTest (Posada, 2008) was used to select the most appropriate model of molecular evolution with Akaike Information Criterion (AIC). Bayesian reconstruction of the data matrix was performed using MrBayes v3.2 (Ronquist and Huelsenbeck, 2003) and the best fitting alternative model GTR+G was adopted. The four Markov chain Monte Carlo (MCMC) chains ran for 5,000,000 generations, sampling every 5,000 generations. The first 10% of burn-in trees were discarded. In order to examine the posterior probability (BPP) of each clade, a majority-rule consensus tree was established.

2.6. Yessotoxin analysis with a usual LC-MS/MS method

Cultures of strain TIO1290 were grown in 200 mL Erlenmeyer flasks under standard culture conditions. At stationary phase, determined via linear regression of log-transformed cell count time series, approximately 10^5 cells were concentrated with a Universal 320 R centrifuge at 850× *g* for 10 min at room temperature. Algal pellets were transferred to 2 mL microcentrifuge tubes and stored at –20°C until analysis for quantification of intracellular YTX.

To extract Yessotoxins (YTXs), 500 µL of methanol and glass beads (150 mg, 100–250 µm in diameter) were added to the pellet. Samples were shaken at 30 Hz for 30 min with MM400 equipment (Mixer Mill MM400, Retsch). After centrifugation at 15,000× *g*, the supernatant was transferred into a 1.5 mL Eppendorf tube. The pellet

was re-extracted with 500 µL of methanol and shaken at 30 Hz for 30 min. After centrifugation at 15,000× *g*, the supernatants were pooled and evaporated to dryness with a gentle flow of nitrogen at 30 °C. The residue was dissolved in 300 µL of methanol, ultrafiltered (0.20 µm, Nanosep MF, Pall) and transferred into an HPLC vial.

Sample analyses were performed by LC-MS/MS using a Shimadzu UFLCxr system coupled to a triple quadruple hybrid mass spectrometer Q-Trap (API400QTrap, Sciex) equipped with a heated electrospray ionization (ESI) source. Data acquisitions were performed using negative ion mode and MRM (Multiple Reaction Monitoring) mode.

Chromatographic separation was carried out on a reversed-phase column Xbridge BEH C18 (50 × 2.1 mm, 2.5 µm, Waters) equipped with a guard column (5 × 2.1 mm, 2.5 µm, same stationary phase as column). Water (A) and acetonitrile 90% (B) both containing 6.7 mM of ammonium hydroxide were used as mobile phases at a flow rate of 400 µL min^{-1}. The following gradient was used: 0 min, 5% B; 1.50 min, 5% B; 4.5 min, 65% B; 5.00 min, 100% B; 7.00 min, 100% B; 7.50 min, 5% B; 12.00 min, 5% B. The oven temperature was 30 °C and the injection volume was 5 µL. The LC-MS/MS methods were used to detect 22 toxins (Table S1). The ESI interface operated using the following parameters: curtain gas 20 psi, temperature: 600 °C, gas1 60 psi; gas2 60 psi, ion spray voltage -4500 V. For detection, the parameters were as follows: the declustering potential was -105 V and the entrance potential -10 V. Two collision energies (Q3_01: -46 eV; Q3_02: -42 eV) and two collision cell exit

potentials (Q3_01: - 9 V; Q3_02: -11 V) were applied and the dwell time was 30 ms. The transitions that were used for the MRM mode are presented in Table S1.

Quantification was performed relative to the YTX standard (National Research Council Canada, NRCC) with a 6-point calibration curve. The limit of detection and quantification was 0.01 and 0.03 ng mL^{-1} for the YTX standard respectively.

2.7. Yessotoxin analysis with an alternative LC-MS/MS method

Some chromatograms were difficult to interpret due to the presence of several peaks and low signal intensities. Moreover, due to the lack of reference material for these toxins, it was not possible to determine with certainty which analogues were actually present in the sample. In an attempt to try to confirm the presence of these toxins, an alternative analytical method was used.

In this alternative method, the chromatographic separation was carried out on a reversed-phase column Kinetex XB-C18 (100 × 2.1 mm, 2.6 µm, Phenomenex) equipped with a guard column. Water (A) and methanol 95% (B) both containing 2 mM ammonium formate and 50 mM formic acid were used as mobile phases at a flow rate of 300 µL min^{-1}. The following gradient was used: 0 min, 30% B; 1.00 min, 70% B; 8.00 min, 85% B; 9.50 min, 100% B; 12.0 min, 100% B; 12.10 min, 30% B; 16.00 min, 30% B. The oven temperature was 40°C and the injection volume was 5 µL. The LC-MS/MS methods were used to detect mono-charged ions of the same 22 toxins (Table S2). The ESI interface operated using the following parameters: curtain gas 20 psi, temperature: 500°C, gas1 40 psi; gas2 60 psi, ion spray voltage -4500 V. For detection, the parameters were as follows: the declustering potential was -155 V and

the entrance potential -10 V. Two collision energies (Q3_01: -100 eV; Q3_02: -48 eV) and two collision cell exit potentials (Q3_01: -19 V; Q3_02: -20 V) were applied and the dwell time was 40 ms. The transitions that were used for the MRM mode are presented in Table S2. Quantification was performed relative to the YTX standard with a 6-point calibration curve. The limit of detection and quantification was respectively 6.7 and 20 ng mL^{-1} for the YTX standard. This alternative method is therefore less sensitive than the usual method.

3. Results

Five strains belonging to three *Gonyaulax* species were obtained by incubating recent sediments from the Adriatic Sea. Two strains were identified as equivalent to *Spiniferites mirabilis* and one strain was related to *S. scabratus.* The other two strains are described as *Gonyaulax montresoriae* sp. nov.

3.1. Morphology

Class: Dinophyceae

Order: Gonyaulacales

Family: Gonyaulacaceae

Genus: Gonyaulax

Gonyaulax montresoriae sp. nov. Shuning Huang, K.N. Mertens & H. Gu

Synonym: *Gonyaulax spinifera* Riccardi et al. 2009, p. 283.

Diagnosis:

Cells were 26–47 µm long and 25–41 µm wide with two short antapical spines. The epitheca was conical with a distinct shoulder on the right. The cell surface was thick and reticulated. The cingulum descended about three times its width and had an overhang of four widths. Cells displayed a plate formula of 2pr, x, 4′, 6″, 6c, 5s, *6‴, 2p, 1⁗. There was a ventral pore at the junction of plates 4′a and 4′p. The angle between the major axis and a line joining the ends of the cingulum was approximately 30°. The cysts of *G. montresoriae* were pear-shaped, 39–53 µm long and 32–45 µm wide. Cysts had a smooth surface and exclusively gonal processes, with low or absent connecting crests. The processes were hollow, 11–15 µm long, with perforations at the base. The archeopyle was reduced, corresponding to plate 3″.

Holotype (designated here): SEM stub of thecate cells from a culture established from a cyst isolated from sediment of Gulf of Trieste, Italy, shown in Fig. 3 and stored at the CEDiT (Centre of Excellence for Dinophyte Taxonomy) dinoflagellate type collection, Wilhelmshaven, Germany with the code CEDiT2024H184.

Type locality: Gulf of Trieste, Italy (45°39′N, 13°36′ E).

Collection date: 12 September 2018 by Xiuyun Cao.

Habitat: Marine and planktonic, with benthic cyst stage.

Etymology: The epithet "*montresoriae*" is in honor of Marina Montresor (born 1956 in Bressanone, Italy), who achieved pioneering work on dinoflagellate cysts in the Mediterranean Sea.

GenBank accession numbers: PQ453139 (SSU rRNA gene), PQ474674 (LSU rRNA gene).

Description:

Cysts of strain TIO1290 were spontaneously produced in culture, even after maintaining it for several years. The cysts were pear-shaped, with a central body with a length of 38.7–52.9 μm (46.4±4.0 μm, n=9) and a width of 32.3–45.3 μm (37.8±4.5 μm, n=7), with a pronounced apical protuberance (Fig. 1A). Cysts had a smooth outer surface and exclusively gonal processes (Fig. 1B, C, E). The processes were hollow, 10.9–14.7 μm long (12.6±1.3 μm, n=10), with perforations at the base (Fig. 1D, F). Crests between processes were low to absent (Fig. 1F). The paracingulum descended with a displacement of three times its width without overhang (Fig. 1C). The processes were trifurcated with bifid terminations (Fig. 1D). The archeopyle was reduced, corresponding to plate 3″ (Fig. 1E, F).

Vegetative cells of strain TIO1290 were 26.2–46.6 μm (35.8±5.5 μm, n=38) long and 24.7–40.7 μm (31.3±5.4 μm, n=38) wide. The epitheca was conical, with a distinct shoulder on the right, and the hypotheca was trapezoidal (Fig. 2A). The cingulum was located in the middle and descended about three times its width with an overhang of four times its width (Fig. 2B). Two unequal antapical spines were generally present, 2.0–7.3 μm (4.4 ± 1.4 μm, n=10) long, but absent in some cells (Fig. 2A, C, D). Occasionally as many as five antapical spines were observed to form a fin (Fig. 2B). The nucleus was elongated and located in the hypocone (Fig. 2E). Numerous bead-like chloroplast lobes were observed (Fig. 2C, F).

Cells of strain TIO1290 had a plate formula of 2pr, x, *4′, 6″, 6c, 5s, *6‴, 2p, 1⁗.

The cells had a typical sexiform gonyaulacoid tabulation with S-type ventral organization and neutral torsion (Fig. 3A, B). Plate 1′ was narrow and elongated, connected to the apical pore complex (apc) through a short x plate, and plate 4′ was divided into 4′a and 4′p, with the ventral pore lying in between (Fig. 3C). Trichocyst pores were evenly distributed on the cell surface (Fig. 3B, C). Plates 2′ and *3′ were large and similar in size. Six precingular plates were present with 1″ and 2″ wide the sixth triangular and smaller (Fig. 3B, D). The apc comprised a cover plate surrounded by a pore plate (Fig. 3E). The cingulum formed approximately 30° angle to the main axis of the cell (Fig. 3A, I). The cingulum comprised of six cingular plates (Fig. 3F). Plate 1p was much smaller than plate 2p (Fig. 3G). The sulcus was composed of anterior sulcal plate (Sa), anterior left sulcal plate (Ssa), posterior left sulcal plate (Ssp), right anterior sulcal plate (Sda) and right posterior sulcal plate (Sdp) (Fig. 3H, I). Schematic plate patterns are provided (Fig. 4). Cells of strain TIO1288 was morphologically close to strain TIO1290.

The cyst of strain TIO1296 resembled *Spiniferites mirabilis*. It was oval, 52.5 μm long and 41.7 μm wide with a pronounced apical protuberance (Fig. 5F). The paracingulum descended with a displacement of three times its width without overhang (Fig. 5A). Processes were hollow and conical, 8.1–14.1 μm (10.5 ± 2.4 μm, n=6) long. There were one or two intergonal processes along each major suture (Fig. 5B, D, E). The archeopyle was reduced, corresponding to plate 3″ (Fig. 5C). Several antapical processes formed a large flange to connect each other (Fig. 5F). The culture

was lost soon so cell morphology was not available. It was tentatively named as *Gonyaulax* sp. 1. Strain TIO1294 was related with *S. scabratus* and tentatively named as *Gonyaulax* sp. 2, but its morphological information was not available.

3.2 Molecular phylogeny

Gonyaulax montresoriae strains TIO1288 and TIO1290 are identical in LSU sequences. They shared 98.21% similarity with a putative *Gonyaulax spinifera* strain GSA0501 from the Adriatic Sea (GenBank accession: EF416284), and 94.22% similarity with a putative *Gonyaulax spinifera* strain GSCQ-1 from Mexico (GenBank accession: JQ638936). *Gonyaulax* sp. 2 strain TIO1294 shared 99.40% similarity with *Spiniferites scabratus* (GenBank accession: MW775711). *Gonyaulax* sp. 1 strain TIO1272 shared 84.86% similarity with *Spiniferites mirabilis* (GenBank accession: MW775699).

Phylogenetic trees of LSU rRNA based on maximum likelihood (ML) and Bayesian inference (BI) are similar. The BI tree showed five well-resolved clades, corresponding to families Ceratiaceae, Protoceratiaceae, Pyrophacaceae, Gonyaulacaceae and Lingulodiniaceae (Fig. 6). Gonyaulacaceae was monophyletic with strong support (BI BPP: 1.0, ML BS: 84) and comprised two clades (clade I and clade II). *Gonyaulax montresoriae* formed a clade with two putative *G. spinifera* from the Adriatic Sea and Mexico with maximal support (BI BPP: 1.0, ML BS: 100). Strain TIO1272 and TIO1294 formed clades with *Spiniferites mirabilis* and *Spiniferites scabratus* with maximal support, respectively. All these strains fell within clade I of Gonyaulacaceae.

Gonyaulax montresoriae strains TIO1288 and TIO1290 were identical in SSU rRNA gene sequences and shared 99.76% similarity to a putative *Gonyaulax spinifera* strain GSA0501 from the Adriatic Sea (GenBank accession: DQ867107). Strains TIO1272 and TIO1296 shared 100% similarity and they shared 97.35% similarity to *Spiniferites mirabilis* (GenBank accession: MW775716). Phylogenetic trees based on SSU rRNA gene sequences (Fig. 7) were similar to those based on LSU rRNA gene sequences.

3.3 Yessotoxin

3.3.1. Analogues detected with the usual LC-MS/MS method

Strain TIO1290 produced yessotoxin and homo-yessotoxin, as well as the potential presence of other analogues. The concentration of YTX was estimated at 2995 ± 150 fg cell^{-1}. Estimation of the homo-yessotoxin concentration was problematic as the signal was very low and interference peaks were present. However, the concentration was estimated to be 0.52 ± 0.002 fg cell^{-1}.

The chromatogram for trinor YTX presented signals at two retention times (RT): 3.4 min and 3.8 min. The chromatograms obtained for 45-OH YTX, COOH YTX, 44-oxotrinor YTX, COOH 45-OH YTX (or 44,55-diOH-41a-HomoYTX) displayed several co-eluted peaks with retention times between 3.5 and 4.5 min. Lastly, Noroxo YTX (or 40-epiNoroxo-YTX or 41-Keto-YTX-1,3-enone) and 44,45 diOH-YTX showed quite intense signals at around 3.8 min. For all these molecules, the ion ratio between the two monitored transitions corresponded to those recorded for yessotoxin.

3.3.2. Analogues potentially detected with an alternative LC-MS/MS method

The chromatogram for trinor YTX displayed a signal on only one of the two transitions (m/z 1101.4 > 1021.4). The signal may have been too weak to be detected on the second transition (m/z 1101.4 > 855.5). The chromatograms obtained for 45-OH YTX and COOH YTX were very noisy, making it difficult to distinguish any signals. Noroxo YTX (or 40-epi Noroxo-YTX or 41-Keto-YTX-1,3-enone) presented a signal whose ion ratio did not correspond to the one obtained for the yessotoxin standard. Both 44-oxotrinor YTX and COOH 45-OH YTX (or 44,55-diOH-41a-Homo-YTX), as well as 44,45 diOH-YTX, showed signals on both transitions with ion ratios similar to those obtained for the yessotoxin standard. Although neither of the two methods used can confirm the presence of the various analogues beyond doubt, several elements are promising. Some analogues show signals with both analytical methods and have ion ratios close to those of yessotoxin: 44-oxotrinor YTX, COOH 45-OH YTX (or 44,55-diOH-41a-Homo-YTX), and 44,45 diOH-YTX. For the other analogues, these two elements are not concordant, either because the signals are too weak, or for other reasons. Despite the uncertainty regarding the presence of these analogues, an estimated concentration was calculated (Table 2).

4. Discussion

Three *Gonyaulax* species were obtained by incubating recent sediments from the Adriatic Sea, and two of them produced cysts in culture. Cysts of strain TIO1290 are morphologically similar to *Spiniferites lazus* in terms of a pear-shaped body, an apical

boss, exclusively gonal processes, and perforations at the base of processes (Reid, 1974; Gurdebeke et al., 2018). However, *Spiniferites lazus* is relatively larger (44–58 μm long vs 39–50 μm), and has a microgranular to microreticulate surface, contrasting with the smooth wall of our cysts. Moreover, the apical boss is faint in *S. lazus* but pronounced in the latter (Table 3). Cysts of strain TIO1290 differ from *Spiniferites rhizophorus* in that the latter has no apical boss (Head and Westphal, 1999), and from *S. septentrionalis* by presence of fenestrations at the base of the processes (Londeix et al., 2018). Four unidentified *Spiniferites* species have been reported in two estuarine Mediterranean bays, and two of them are also pear-shaped (Satta et al., 2013); however, the lack of morphological details makes it impossible to compare them with our cysts. Therefore, this is likely a new *Spiniferites* species that will be described in the future, pending further observations.

Cysts of strain TIO1296 are morphologically similar to *S. mirabilis* subsp. *mirabilis* in terms of an antapical flange and one or two intergonal processes. However, its process length (8.1–14.1 μm) appears to be intermediate between *S. mirabilis* subsp. *mirabilis* (15–22 μm) and *S. mirabilis* subsp. *serratus* (7–9 μm) (Limoges et al., 2018). *S. mirabilis* subsp. *mirabilis* is commonly found in the western Mediterranean but is much less common in the eastern Mediterranean (Aydın et al., 2011). An isolate (20–188) from Bahía de La Paz, Gulf of California, is close to *S. mirabilis* subsp. *mirabilis* but smaller (35 μm long vs 40–70 μm; Table 3) (Gu et al., 2021). Biological information on *S. mirabilis* is very limited, including the morphology of motile cells and molecular sequences, and will help to understand the

relationship among these cysts. The culture of strain TIO1294 was lost soon after, but we managed to obtain its LSU sequence, which is nearly identical to that of strain TIO706 from Corsica and identified as equivalent to *Spiniferites scabratus* (Gu et al., 2021). This finding highlight the rich diversity and wide distribution of *Spiniferites* in the Mediterranean Sea.

Cells of strain TIO1290 displayed the plate formula of 2pr, x, 4′, 6″, 6c, 5s, *6‴, 2p, 1⁗, thus fitting the emended description of *Gonyaulax* (Carbonell-Moore et al., 2022). However, a small x plate connecting the apc and plate 1′ was recognized, which has been illustrated but previously overlooked, including *Gonyaulax nezaniae* (Fig. 18 in Gu et al., 2021) and *Gonyaulax kunsanensis* (Fig. 34 in Shin et al., 2024), suggesting that this is a common feature of *Gonyaulax*.

Cells of strain TIO1290 have two antapical spines of unequal size, thus may thus be classified within the *G. spinifera* complex (Kofoid, 1911). Strain TIO1290 has a much higher cingular displacement and overhang (3.0 and 4.0) than *G. spinifera* (equivalent of *Spiniferites ramosus*, 1.0 and 1.0), and longer antapical spines (2.0–7.3 vs 1.2–5.1 µm). Moreover, the antapical spines can be finned sometimes in the former but not in the latter (Gu et al., 2021). Strain TIO1290 differs from *G. pospelovana* in the cingulum displacement and overhang (3.0 and 4.0 vs 2.0 and 2.0), and longer antapical spines (2.0–7.3 vs 1.0–3.0 µm) (Gu et al., 2024). Strain TIO1290 also differs from *G. nezaniae* in that the latter possesses two lengthy and stout antapical spines (2–11 µm) (Gu et al., 2021). A comparison of strain TIO1290 with closely related species is listed in Table 4. In light of the morphological differences of strain

TIO1290 from previously described species, we erect *Gonyaulax montresoriae* sp. nov.

Strain GSA0501 isolated from the Adriatic Sea in May 2005, is probably conspecific with *G. montresoriae* as it shares 98.21% similarity in its LSU sequence with strain TIO1290. Moreover, both strains produce predominantly YTX (Riccardi et al., 2009). However, morphological information of strain GSA0501 is not available, thus more detailed work is needed in the future. The complete 18S rRNA gene sequence of strain TIO1290 was submitted to https://oba.mio.osupytheas.fr to search for *G. montresoriae* from the Tara Oceans 18S V4 metabarcoding data. Unfortunately, no homologous metabarcode sequence matching the submitted sequence was obtained, suggesting that it has a restricted distribution in the Mediterranean Sea. We also failed to detect it in the Mediterranean survey dataset, probably because sampling in the Mediterranean Sea was conducted from September to December, 2009 (Tara Oceans Consortium and Tara Oceans Expedition, 2015), which may have missed *G. montresoriae*, which tends to appear in May (Riccardi et al., 2009).

Our molecular phylogeny, supported by newly obtained sequences, confirms the previous notion that Gonyaulacaceae comprises two clades (Gu et al., 2024). Both toxic and nontoxic species are scattered across either clade, suggesting that YTX production is not systematically significant. On the other hand, cysts of *G. montresoriae* are characterized by fenestrate process bases, shared with *Spiniferites lazus* (Reid, 1974; Gurdebeke et al., 2018), *Spiniferites bentorii* (Gu et al., 2021) and *Spiniferites hainanensis* (Sun and Song, 1992). However, these species are

phylogenetically distant as well, although molecular sequences of *S. hainanensis* are still not available.

Gonyaulax montresoriae strain TIO1290 from the Adriatic Sea produces predominantly YTX of 3.0 pg cell^{-1}, much lower than strain GSA0501 from the same area, which produced 9.3 pg cell^{-1}. Strain GSA0501 produces only YTX and other known YTX analogues such as homoYTX, 45-OHYTX, and 45-OH homoYTX were not detected (Riccardi et al., 2009). None of both methods used here can confirm the presence of the various analogues with certainty; however, several elements are promising. Some analogues show signals with both analytical methods and have ion ratios close to those of yessotoxin: 44-oxotrinor YTX, COOH 45-OH YTX (or 44,55-diOH-41a-Homo-YTX), 44, 45 diOH-YTX. For the other analogues, these two elements are not concordant, likely because the signals are too weak. Due to the lack of reference material for these toxins, it was not possible to determine with certainty which analogues were present in the sample. However, high-resolution LC/MS analyses could clarify any doubts.

It is well known that three dinoflagellate species — *Lingulaulax polyedra, Protoceratium reticulatum* and *G. spinifera* — are able to produce YTXs (Paz et al., 2008). *Lingulaulax polyedra* is considered a species displaying low toxicity species compared to the other two (Peter et al., 2018). In fact, different batch cultures of a *L. polyedra* strain from the Adriatic Sea produce YTXs less than 0.1 pg cell^{-1} (Pistocchi et al., 2012). In contrast, several Adriatic strains of *P. reticulatum* produce YTXs ranging from 4.5 to 65.0 pg cell^{-1} (Guerrini et al., 2007). Two strains of putative *G.*

spinifera from the Adriatic Sea have been reported to produce 5.4 and 33.4 pg cell^{-1} of YTXs (Riccardi et al., 2009), and one of them is identified as *G. montresoriae* here, suggesting that *Protoceratium reticulatum* and *G. montresoriae* are major contributors to YTXs contamination in Adriatic Sea shellfish.

YTXs were first detected in mussels from the northeastern Adriatic Sea in 1995 (Ciminiello et al., 1997). Monitoring of potential YTX producer has intensified since. *Lingulaulax polyedra* was dominant from 2012 to 2017, when the density of *G. spinifera* did not exceed 200 cell L^{-1}. However, *G. spinifera* (probably *G. montresoriae*) became abundant (>500 cell L^{-1}) in May of 2017, 2018 and 2019, accompanied by a sharp increase in toxin levels and the closure of mussel farms (Rubini et al., 2021). *Gonyaulax montresoriae* wasfirst oberved in May 2005 (Riccardi et al., 2009), when water temperatures were around 18 °C. This temperature persisted for longer periods due to global warming (Rubini et al., 2021; Bonacci and Vrsalović, 2022), increasing the risk of YTX contamination in cultured mussels in this area.

The Adriatic isolate GSA0602, sampled in October 2006, predominantly produces Homo-YTX and is genetically close to two putative *G. spinifera* strains from New Zealand (Riccardi et al., 2009). These New Zealand strains tested positive for YTXs by ELISA, and one strain even produced cysts resembling *Spiniferites mirabilis* (Rhodes et al., 2006). Further investigation is required to confirm the identities of these strains. YTX production by other *Gonyaulax* species, such as those

equivalent to *S. mirabilis* and *S. scabratus*, has not yet been examined and will be the focus of future study.

Acknowledgements

This work was supported by the National Natural Science Foundation of China (42076085, 42030404). KNM and OD was financially supported by the French National Research Agency (ANR) PhenoMap project, ANR-20-CE02-0025 and the project ORDINAR (ANR-22-CE01-0010).

REFERENCES

Álvarez, G., Uribe, E., Regueiro, J., Blanco, J., Fraga, S., 2016. *Gonyaulax taylorii*, a new yessotoxins-producer dinoflagellate species from Chilean waters. Harmful Algae 58, 8–15.

Armstrong, M., Kudela, R., 2006. Evaluation of California isolates of *Lingulodinium polyedrum* for the production of yessotoxin. Afr. J. Mar. Sci. 28(2), 399 – 401.

Aydın, H., Matsuoka, K., Minareci, E., 2011. Distribution of dinoflagellate cysts in recent sediments from Izmir Bay (Aegean Sea, Eastern Mediterranean). Mar. Micropaleontol. 80(1), 44 – 52.

Bonacci, O., Vrsalović, A., 2022. Differences in Air and Sea Surface Temperatures in the Northern and Southern Part of the Adriatic Sea. Atmosphere 13(7), 1158.

Carbonell-Moore, M.C., Matsuoka, K., Mertens, K.N., 2022. Gonyaulacalean tabulation revisited using plate homology and plate overlap, with emphasis on the

ventral area (Dinophyceae). Phycologia 61(2), 195 – 210.

Chikwililwa, C., McCarron, P., Waniek, J.J., Schulz-Bull, D.E., 2019. Phylogenetic analysis and yessotoxin profiles of *Gonyaulax spinifera* cultures from the Benguela Current upwelling system. Harmful Algae, 101626.

Ciminiello, P., Fattorusso, E., Forino, M., Magno, S., Poletti, R., Satake, M., Viviani, R., Yasumoto, T., 1997. Yessotoxin in mussels of the northern Adriatic Sea. Toxicon 35(2), 177 – 183.

Ciminiello, P., Fattorusso, E., Forino, M., Magno, S., Poletti, R., Viviani, R., 1998. Isolation of adriatoxin, a new analogue of yessotoxin from mussels of the Adriatic Sea. Tetrahedron Lett. 39(48), 8897 – 8900.

Dodge, J., 1989. Some revisions of the family Gonyaulacaceae (Dinophyceae) based on a scanning electron microscope study. Bot. Mar. 32(4), 275–298.

Domínguez, H.J., Souto, M.L., Norte, M., Daranas, A.H., Fernández, J.J., 2010. Adriatoxin-B, the first C13 terminal truncated YTX analogue obtained from dinoflagellates. Toxicon 55(8), 1484 – 1490.

Ellegaard, M., Daugbjerg, N., Rochon, A., Lewis, J., Harding, I., 2003. Morphological and LSU rDNA sequence variation within the *Gonyaulax spinifera-Spiniferites* group (Dinophyceae) and proposal of *G. elongata* comb. nov. and *G. membranacea* comb. nov. Phycologia 42(2), 151–164.

Gu, H., Huo, K., Krock, B., Bilien, G., Pospelova, V., Li, Z., Carbonell-Moore, C., Morquecho, L., Ninčević, Ž., Mertens, K.N., 2021. Cyst-theca relationships of *Spiniferites bentorii*, *S. hyperacanthus*, *S. ramosus*, *S. scabratus* and molecular

phylogenetics of *Spiniferites* and *Tectatodinium* (Gonyaulacales, Dinophyceae). Phycologia 60(4), 332–353.

Gu, H., Mertens, K.N., Derrien, A., Bilien, G., Li, Z., Hess, P., Séchet, V., Krock, B., Amorim, A., Li, Z., Pospelova, V., Smith, K.F., MacKenzie, L., Yoon, J.Y., Kim, H.J., Shin, H.H., 2022. Unravelling the *Gonyaulax baltica* species complex: Cyst-theca relationship of *Impagidinium variaseptum*, *Spiniferites pseudodelicatus* sp. nov. and *S. ristingensis* (Gonyaulacaceae, Dinophyceae), with descriptions of *Gonyaulax bohaiensis* sp. nov, *G. amoyensis* sp. nov. and *G. portimonensis* sp. nov. J. Phycol. 58(3), 465–486.

Gu, H., Zheng, J., Huang, S., Morquecho, L., Krock, B., Shin, H.H., Li, Z., Derrien, A., Mertens, K.N., 2024. A new dinoflagellate *Gonyaulax pospelovana* with resting cysts resembling *Spiniferites delicatus* and its biogeography and ecology revealed by DNA metabarcoding. Phycologia 63(1), 74–88.

Guerrini, F., Ciminiello, P., Dell'Aversano, C., Tartaglione, L., Fattorusso, E., Boni, L., Pistocchi, R., 2007. Influence of temperature, salinity and nutrient limitation on yessotoxin production and release by the dinoflagellate *Protoceratium reticulatum* in batch-cultures. Harmful Algae 6(5), 707–717.

Gurdebeke, P.R., Mertens, K.N., Bogus, K., Marret, F., Chomérat, N., Vrielinck, H., Louwye, S., 2018. Taxonomic re-investigation and geochemical characterization of Reid's (1974) species of *Spiniferites* from holotype and topotype material. Palynology 42(sup1), 93–110.

Hall, T.A., 1999. BioEdit: A User-Friendly Biological Sequence Alignment Editor and

Analysis Program for Windows 95/98/NT. Nuclc Acids Symposium Series 41(41), 95–98.

Head, M. J., Westphal, H. 1999. Palynology and paleoenvironments of a Pliocene carbonate platform: the Clino Core, Bahamas. J. Paleontol. 73(1), 1–25.

Head, M. J., Mertens, K. N., & Fensome, R. A. 2024. Dual nomenclature in organic-walled dinoflagellate cysts I: concepts, methods and applications. Palynology 48(2), 2290200.

Katoh, K., Standley, D.M., 2013. MAFFT multiple sequence alignment software version 7: improvements in performance and usability. Mol. Biol. Evol. 30(4), 772–780.

Kim, H.J., Li, Z., Gu, H., Mertens, K.N., Yeon Youn, J., Yoon Kwak, K., Oh, S.-J., Shin, K., Yoo, Y.D., Lee, W., 2022. *Gonyaulax geomunensis* sp. nov. and two allied species (Gonyaulacales, Dinophyceae) from Korean coastal waters and East China Sea: morphology, phylogeny and growth response to changes in temperature and salinity. Phycologia 62(1), 48–67.

Kofoid, C.A., 1911. Dinoflagellata of the San Diego region, IV. The genus *Gonyaulax* with notes on its skeletal morphology and a discussion of its generic and specific characters. University of California Publication in Zoology 8, 187–286.

Londeix, L., Zonneveld, K., Masure, E. 2018. Taxonomy and operational identification of Quaternary species of *Spiniferites* and related genera. Palynology 42(sup1), 45–71.

Liang, Y., Zhong, Y., Xi, Y., He, L., Zhang, H., Hu, X., Gu, H., 2024. Toxic effects of combined exposure to homoyessotoxin and nitrite on the survival, antioxidative responses, and apoptosis of the abalone *Haliotis discus* hannai. Ecotoxicol. Environ.

Saf. 272, 116058.

Limoges, A., Londeix, L., Mertens, K.N., Rochon, A., Pospelova, V., Cuéllar, T., de Vernal, A., 2018. Identification key for Pliocene and Quaternary *Spiniferites* taxa bearing intergonal processes based on observations from estuarine and coastal environments. Palynology 42(sup1), 72 – 88.

Mertens, K.N., Aydin, H., Uzar, S., Takano, Y., Yamaguchi, A., Matsuoka, K., 2015. Relationship between the dinoflagellate cyst *Spiniferites pachydermus* and *Gonyaulax ellegaardiae* sp. nov. from Izmir Bay, Turkey, and molecular characterization. J. Phycol. 51, 560–573.

Miles, C.O., Wilkins, A.L., Hawkes, A.D., Selwood, A.I., Jensen, D.J., Munday, R., Cooney, J.M., Beuzenberg, V., 2005. Polyhydroxylated amide analogs of yessotoxin from *Protoceratium reticulatum*. Toxicon 45(1), 61 – 71.

Murata, M., Kumagai, M., Lee, J.S., Yasumoto, T., 1987. Isolation and structure of yessotoxin, a novel polyether compound implicated in diarrhetic shellfish poisoning. Tetrahedron Lett. 28(47), 5869 – 5872.

Paz, B., Daranas, A.H., Norte, M., Riobó, P., Franco, J.M., Fernández, J.J., 2008. Yessotoxins, a group of marine polyether toxins: an overview. Mar. Drugs 6(2), 73 – 102.

Peter, C., Krock, B., Cembella, A., 2018. Effects of salinity variation on growth and yessotoxin composition in the marine dinoflagellate *Lingulodinium polyedra* from a Skagerrak fjord system (western Sweden). Harmful Algae 78, 9 – 17.

Pistocchi, R., Guerrini, F., Pezzolesi, L., Riccardi, M., Vanucci, S., Ciminiello, P.,

Dell'Aversano, C., Forino, M., Fattorusso, E., Tartaglione, L., 2012. Toxin levels and profiles in microalgae from the North-Western Adriatic Sea—15 years of studies on cultured species. Mar. Drugs 10(1), 140 – 162.

Pitcher, G.C., Foord, C.J., Macey, B.M., Mansfield, L., Mouton, A., Smith, M.E., Osmond, S.J., van der Molen, L., 2019. Devastating farmed abalone mortalities attributed to yessotoxin-producing dinoflagellates. Harmful Algae 81, 30–41.

Posada, D., 2008. jModelTest: Phylogenetic Model Averaging. Mol. Biol. Evol. 25(7), 1253 – 1256.

Reid, P., 1974. Gonyaulacacean dinoflagellate cysts from the British Isles. Nova Hedwig 25, 579–637.

Rhodes, L., McNabb, P., De Salas, M., Briggs, L., Beuzenberg, V., Gladstone, M., 2006. Yessotoxin production by *Gonyaulax spinifera*. Harmful Algae 5(2), 148–155.

Riccardi, M., Guerrini, F., Roncarati, F., Milandri, A., Cangini, M., Pigozzi, S., Riccardi, E., Ceredi, A., Ciminiello, P., Dell'Aversano, C., 2009. *Gonyaulax spinifera* from the Adriatic sea: Toxin production and phylogenetic analysis. Harmful Algae 8(2), 279–290.

Rochon, A., Lewis, J., Ellegaard, M., Harding, I.C., 2009. The *Gonyaulax spinifera* (Dinophyceae) "complex": Perpetuating the paradox? Rev. Palaeobot. Palynol. 155(1), 52–60.

Ronquist, F., Huelsenbeck, J.P., 2003. MrBayes 3: Bayesian phylogenetic inference under mixed models. Bioinformatics 19(12), 1572 – 1574.

Rubini, S., Albonetti, S., Menotta, S., Cervo, A., Callegari, E., Cangini, M., Dall'Ara,

S., Baldini, E., Vertuani, S., Manfredini, S., 2021. New trends in the occurrence of yessotoxins in the Northwestern Adriatic Sea. Toxins 13(9), 634.

Ryther, J.H., Guillard, R.R.L., 1962. Studies of Marine Planktonic Diatoms: Iii. Some Effects of Temperature on Respiration of Five Species. Can. J. Microbiol. 8(4), 447–453.

Satta, C.T., Anglès, S., Lugliè, A., Guillén, J., Sechi, N., Camp, J., Garcés, E., 2013. Studies on dinoflagellate cyst assemblages in two estuarine Mediterranean bays: A useful tool for the discovery and mapping of harmful algal species. Harmful Algae 24, 65–79.

Shin, H.H., Li, Z., Mertens, K.N., Yoo, Y.D., Youn, J.Y., Lee, M., Gu, H., 2024. Morphology and molecular phylogeny of *Gonyaulax kunsanensis* sp. nov. (Gonyaulacales, Dinophyceae) from Korean coastal waters. Bot. Mar. https://doi.org/10.1515/bot-2023-0106.

Silvestro, D., Michalak, I., 2012. raxmlGUI: a graphical front-end for RAxML. Org. Divers. Evol. 12, 335–337.

Sun, X., Song, Z., 1992. Quaternary dinoflagellates from Arenaceous Dolomite in Hainan Island. Acta Micropalaeontologica Sinica 9(1), 45–52.

Tara Oceans Consortium, C., Tara Oceans Expedition, P., 2015. Registry of all stations from the Tara Oceans Expedition (2009-2013). PANGAEA.

Fig. 1. Light (LM) and scanning electron micrographs (SEM) of cysts produced in culture of strain TIO1290. (A) LM, a living cyst in ventral view, showing the apical boss (arrow) and cell contents surrounded by an endospore. (B) SEM, a living cyst in dorso-antapical view. (C) SEM, cyst in ventral view, showing the cingulum (arrows). (D) SEM, a gonal trifurcate process with bifid distal ends. (E) SEM, a living cyst in dorsal view. (F) SEM, a living cyst in dorsal view, showing the reduced archeopyle and fenestrate bases of the processes (arrows).

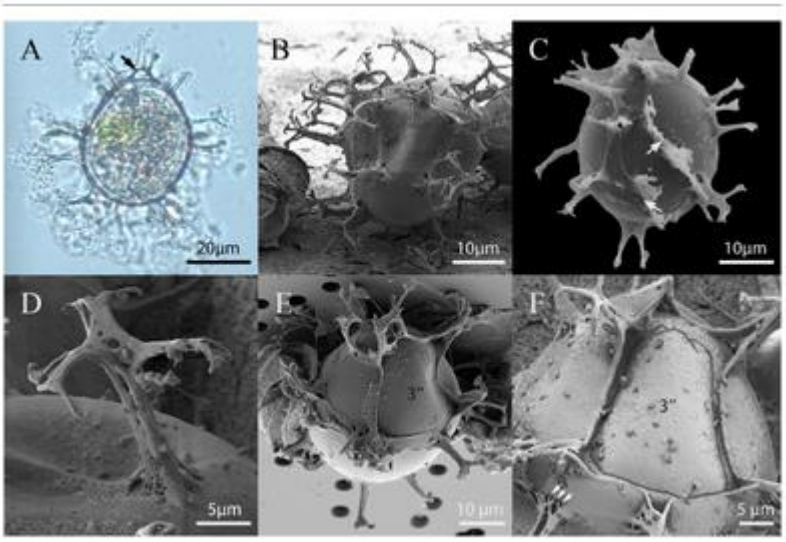

Fig. 2. Light micrographs (LM) of cells of strain TIO1290. (A) A living cell in ventral view, showing the pronounced shoulder. (B) A living cell in ventral view, showing the cingular displacement. (C) A living cell in dorsal view, showing the chloroplast lobes. (D) A living cell in mid-focus, showing two antapical spines (arrows). (E) A SYBR Green-stained cell, showing the elongated nucleus (N). (F) A SYBR Green-stained cell, showing the thick nucleus (N) and chloroplast lobes.

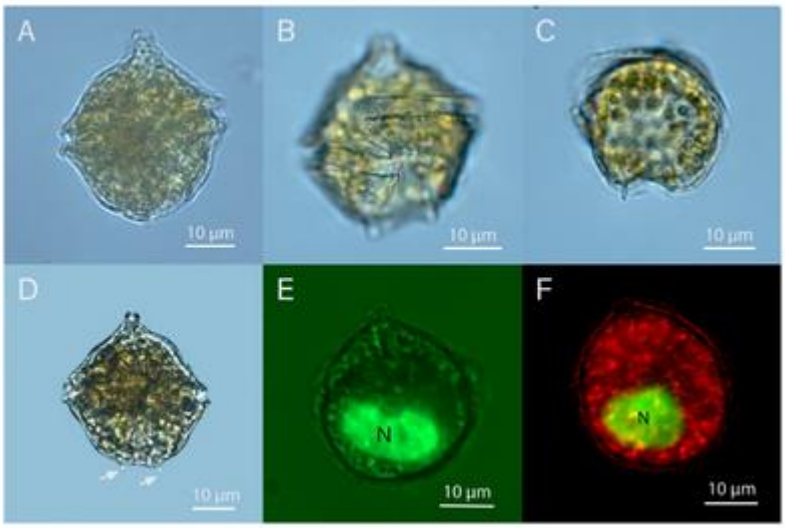

Fig. 3. Scanning electron micrographs (SEM) of cells of strain TIO1290. (A) Ventral view of a cell showing cingular displacement, two antapical spines and the anterior sulcal plate (Sa). (B) Dorsal view of a cell showing two precingular plates (3″–4″) and two postcingular plates (*4‴–*5‴). (C) Ventral view of a cell showing the x plate, a ventral pore between plates 4′a and 4′p. (D) Apical view of a cell showing two apical plates (2′, *3′) and six precingular plates (1″–6″). (E) Apical view of a cell illustrating the apical pore complex (apc). (F) A broken cell showing six cingular plates (1c–6c). (G) Antapical view of a cell showing five postcingular plates (*2‴–*6‴), one antapical plate (1⁗) and two posterior intercalary plates (1p, 2p). (H, I) Ventral views showing the left anterior sulcal plate (Ssa), left posterior sulcal plate (Ssp), anterior right sulcal plate (Sda), and posterior right sulcal plate (Sdp).

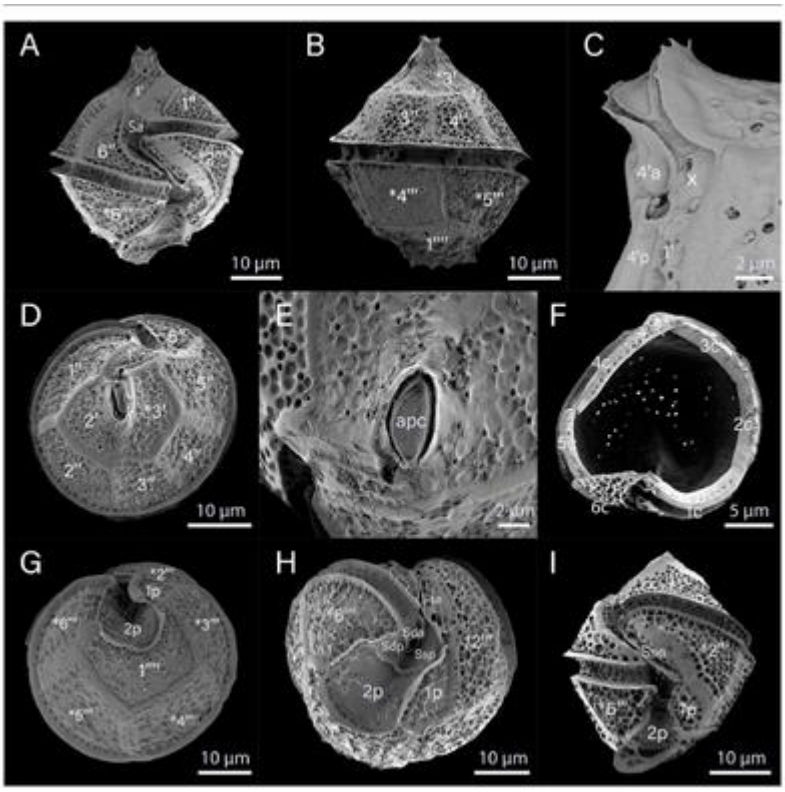

Fig. 4. Schematic drawing of *Gonyaulax montresoriae*. (A) Ventral view. (B) Dorsal view. (C) Apical view. (D) Antapical view.

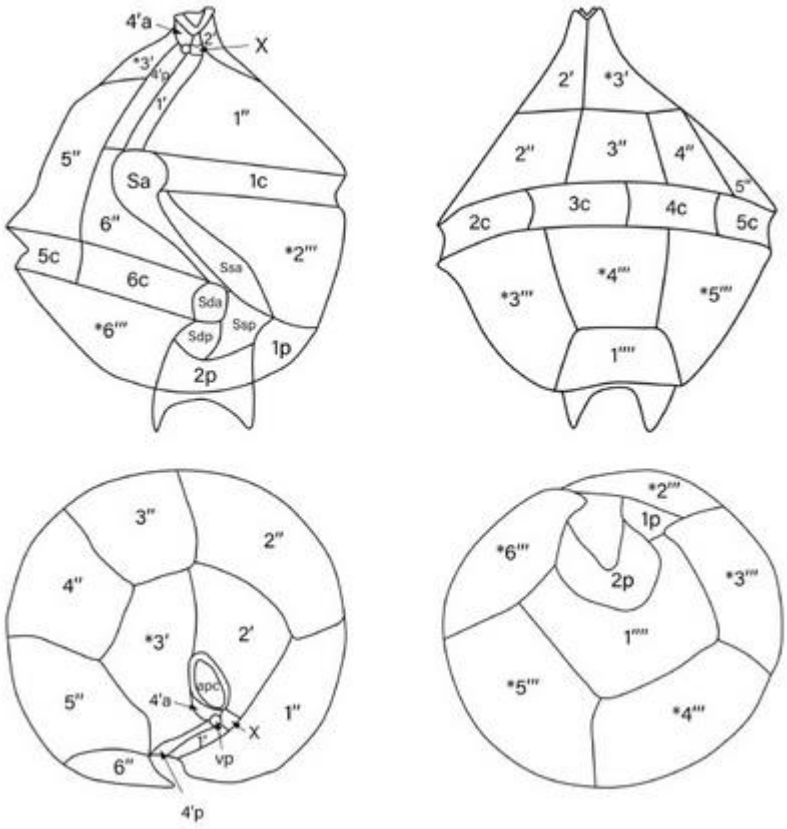

Fig. 5. Light micrographs (LM) of an empty cyst produced in culture of strain TIO1296. (A) Ventral view, showing the cingulum (arrows). (B) Lateral view, showing an intergonal process (arrow). (C) Dorsal view, depicting the archeopyle. (D) Dorsal view, illustrating the intergonal processes. (E) Antapical view, showing two posterior intercalary plates (1p, 2p). (F) Mid-focus, showing the apical boss (arrow) and antapical flange.

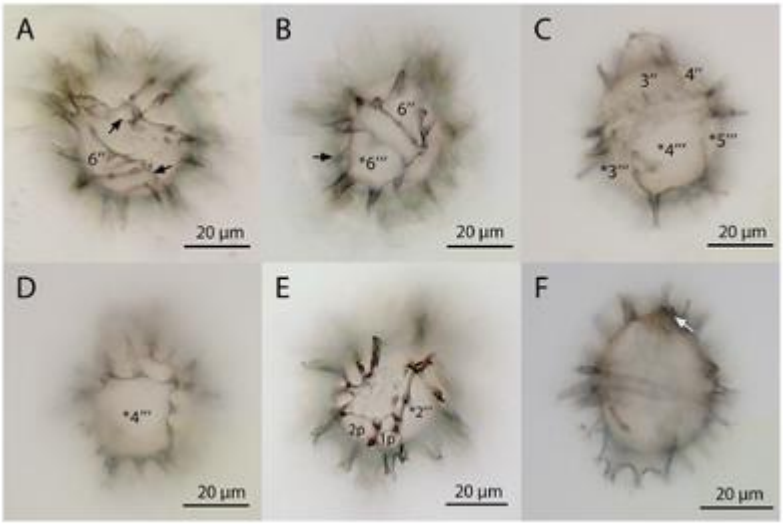

Fig. 6. Molecular phylogeny of *Gonyaulax* inferred from partial LSU rRNA gene sequences based on Bayesian inference (BI). *Adenoides eludens* (GenBank accession: LC002845) was used as outgroup. New sequences are shown in bold red. Numbers at nodes represent Bayesian posterior probabilities and the ML bootstrap values,∗ indicate the maximal support in 100% ML bootstrap support and 1.00 Bayesian posterior probabilities. Bootstrap values > 50% and posterior probabilities > 0.90 are shown. Branch lengths drawn to scale, with the scale bar indicating the number of nucleotide substitutions per site.

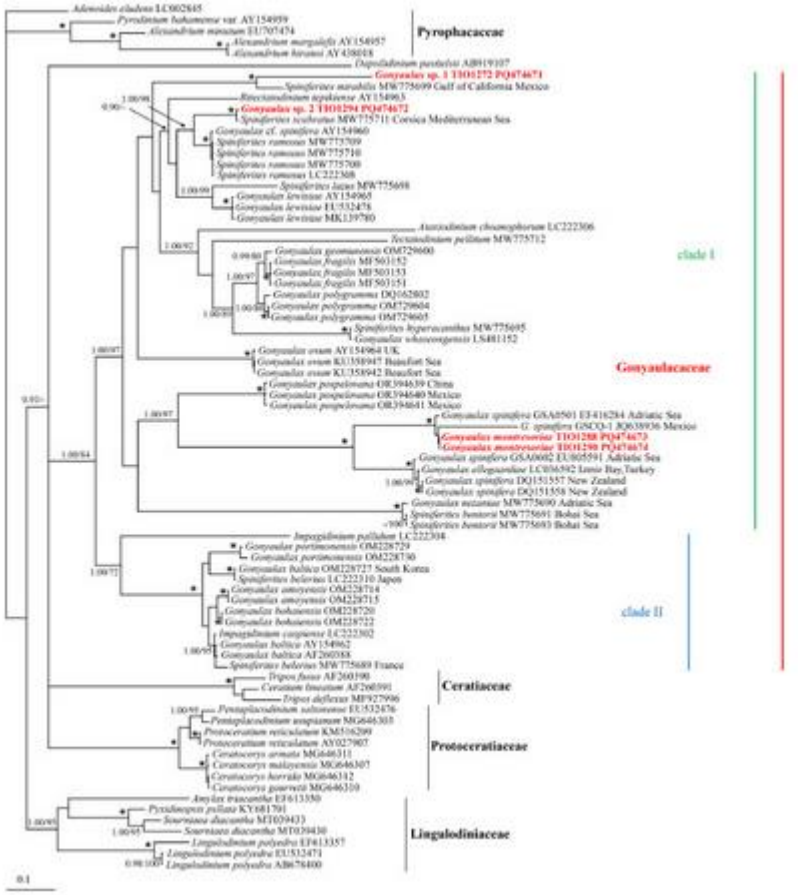

Fig. 7. Molecular phylogeny of *Gonyaulax* inferred from partial SSU rRNA gene sequences based on Bayesian inference (BI). *Adenoides eludens* (GenBank accession: EF492484) was used as outgroup. New sequences are shown in bold red. Numbers at nodes represent Bayesian posterior probabilities and the ML bootstrap values,∗ indicate the maximal support in 100% ML bootstrap support and 1.00 Bayesian posterior probabilities. Bootstrap values > 50% and posterior probabilities > 0.90 are shown. Branch lengths drawn to scale, with the scale bar indicating the number of nucleotide substitutions per site.